16th ICAAR LISBOA 2020-2022

16th International Conference on
Alkali-Aggregate Reaction in Concrete
Lisboa | LNEC | Portugal | 31 May - 2 June 2022

http://icaar2020-2022.lnec.pt

ASR modelling: 3D microstructure reconstruction of reactive aggregate from 2D images

Xiujiao Qiu [(1)], Maxim Deprez [(2)], Guang Ye [(3)], Geert De Schutter[(4)]

(1) Department of Structural Engineering and Building Materials, Ghent University, Ghent, Belgium, Xiujiao.qiu@ugent.be

(2) PProGRess/UGCT, Geology Department, Ghent University, Ghent, Belgium, Maxim.Deprez@ugent.be

(3) Department of Materials, Mechanics, Management & Design, Delft University of Technology, 2628 CN Delft, The Netherlands, G.Ye@tudelft.nl

(4) Department of Structural Engineering and Building Materials, Ghent University, 9052 Ghent, Belgium, Geert.DeSchutter@ugent.be

Abstract

The reactive silica distribution in the aggregate plays a significant role in alkali silica reaction (ASR) in concrete, as it affects the localization of the ASR products as well as the following structural mechanical response. However, the microstructure of aggregate was either simplified or neglected in the current ASR models because of the difficulty to obtain a representative microstructure at a desired spatial resolution. In order to fill this gap, this paper proposed a model that simulates the 3D microstructure of an alkali-reactive aggregate from 2D images. Based on 2D images, the ASR related phase fractions (reactive silica) and their autocorrelation functions (ACF) of a siliceous limestone were first calculated through image analysis. By utilizing Gaussian filtering method and the calculated ACF, five representative 3D microstructures with different quartz fractions were simulated from the selected 2D images. The striking visual similarity and well-fitting of the autocorrelation functions for the distance up to 10 pixels shows that this method has a good ability to reconstruct the real 3D microstructure based on the 2D image. The simulated microstructures can be applied for a multiscale ASR simulation to simulate the chemical reaction as well the physical response at microscale.

***Keywords**: ASR; reactive silica phases; 3D microstructure; two-point probability function*

1. INTRODUCTION

The whole ASR process evolves at different scales. At microscale the chemical reaction happens between the pore solution in the cement paste and the reactive silica in the aggregate, while the physical fracture begins at low scale and extends to the whole structure at macroscale [1]. At microscale, the microstructure of aggregate plays a significant role behind the ASR mechanism, not only because it provides the reaction sites but also it determines the cracking pattern. According to the research of Ponce and Batic [2], the cracking pattern of ASR-affected concrete depends on the mineralogical nature of the aggregate. For rapid-reacting aggregates containing amorphous silica such as opal and vitreous volcanic rocks, ASR product formation and expansion happen at the paste-aggregate interface transition zone (ITZ). However, for slow-reacting aggregates containing defected crystal quartz such as siliceous limestone, the gel occurrence and expansion come mainly from the inside of the aggregate. Leemaan et.al [3] also confirmed this phenomenon by adding caesium in concrete to track the ASR sequence.

Modelling is needed to analyse and predict the behaviour of ASR-affected structures, thus evaluating the safety level, providing suggestions about the strengthening of degraded structures, and also in view of preventative measures for to-be-built structures. Present ASR simulation models mostly focus at mesoscale or macroscale. In these models, the aggregates are either being taken as homogeneous such that the cracking is caused by the product accumulation in the ITZ [4,5] or the expansive sites are distributed inside aggregates randomly [6]. The chemical reaction is simplified to a kinetic raw that only considers few influencing factors of ASR. These models are able to provide a good prediction about the pessimum size of aggregate or the structural mechanical degradation. However, the crack development at different scales (for example how the crack at microscale affects the cracking at mesoscale) as well as the different cracking pattern that depending on the mineralogy of the aggregate cannot be captured

by these models. Furthermore, due to the simplification of the chemical reaction mechanism in these models they couldn't provide a detailed explanation about what happened to the materials behind the cracking. A model which can derive the fracture mechanism at different scales from the chemical reaction simulation is the future of ASR modelling [7]. The multiscale technique can be adopted to construct such a model since it facilitates both down and upscaling to reaction products and structural level respectively. The microstructure of aggregate then becomes a necessity to be considered in such a multiscale model for the simulation of the chemical reaction.

The best microstructure model is definitely the digitized three-dimensional (3D) representation of real aggregate obtained through CT scan. However, it is not often used as limited by the resolution, especially for the ASR reactive aggregate whose representative volume is at centimetre scale while the reactive silica particle size inside may vary from nanometer to a few hundred micrometer. Although not as perfect as the best model, reconstructed microstructure are widely used as they can be built from information obtained from 2D micro-images which are easily available. A number of reconstruction approaches have been developed [8-10] and among them the Gaussian filtering method and simulated annealing method were extensively examined. The Gaussian filtering method has been used and extended by Bentz [11] to reconstruct the 3D representation of cement matching the phase volume fractions and surface-area fractions of the 2D images. Based on his experience, Gaussian filtering method is introduced in this paper to reconstruct the 3D microstructure of limestone considering the pore and reactive silica distribution. Due to the random distribution of the reactive silica, five different microstructures with different reactive silica fractions were reconstructed. The simulated microstructure of the limestone is compared visually (phase distribution characteristics) and numerically with the original 2D images, The simulated microstructures can used in a comprehensive ASR model for chemical reaction as well as physical response simulation.

2. 2D MORPHOLOGICAL INFORMATION OF A LIMESTONE

2.1 Reactive silica phases

ASR is one of the serious durability problem in Belgium which costs a huge economic loss to repair the affected structure. A siliceous limestone in Belgium is discovered to be very ASR reactive [19]. To study the mineral composition of the limestone, six thin sections were firstly obtained using an automatic thin section machine in Magnel-Vandepitte laboratory of Ghent University. A representative test sample of around 1 kg was firstly obtained from the bulk sample conforming to [12]. The test sample was then dried at 40°C until a constant weight was reached. Last, the test sample was impregnated with epoxy resin. Then six standard petrographic thin sections 28 × 48 mm were prepared from the test sample. The typical optical micrographs of limestone are shown in Figure 2.1.

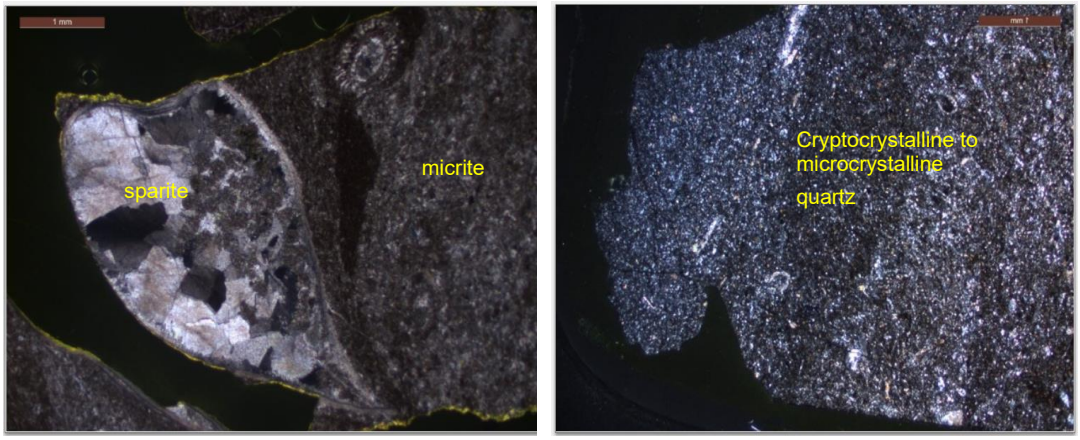

(a) (b)

Figure 2.1: Silica phases in limestone under XPL: (a) Well-crystallized quartz replaced part of the matrix; (b) Cryptocrystalline to microcrystalline quartz matrix.

The minerals composing the limestone were identified based on their optical properties as illustrated in [20]. The limestone is mainly composed of micrite (microcrystalline calcite ($CaCO_3$) with a crystal size less than 5 μm, sparite (calcite with crystal size bigger than 64 μm) as shown in Figure 2.1 (a) and

interspersed microcrystalline and cryptocrystalline quartz (SiO_2) as shown in Figure 2.1(b). According to [17], the reactive silica phase in the limestone is cryptocrystalline to microcrystalline quartz. The relative mass fraction of the different phases are determined using XRD as described below.

2.2 XRD analysis of the limestone

Three representative samples around 9 g for X-ray diffraction (XRD) test are obtained from the bulk samples according to the standard EN 932-2 [12]. 1g zincite was added into each sample. XRD measurements were carried out by using a Thermo Scientific ARL X'tra Diffractometer equipped with a Peltier cooled detector, operated at 40Kv and 35 mA using CuK α from 5^o to 75^o 2θ at 0.02 2θ increments with 1 s counting time increment. The quantitative mineral volume composition results are calculated based on the mass composition and are shown in Table 2.1. It can be seen that except calcite ($CaCO_3$) and quartz (SiO_2), there are also small portions of dolomite CaMg $(CO_3)_2$, and fluorite (CaF_2), which is not easy to be found in the thin section. The average quartz volume percentage is 13.21%. This volume percentage is used as one of the references to choose different SEM-BSE images for 3D microstructure reconstruction as stated in the next section.

Table 2.1: The quantitative mineral volume composition of limestone.

Minerals	Calcite,%	Dolomite,%	Quartz, %	Fluorite,%
Sample 1	78.26	6.84	12.37	2.54
Sample 2	78.34	5.53	13.69	2.44
Sample 3	79.51	4.19	13.58	2.71
Average,%	78.70	5.52	13.21	2.56

2.3 2D microstructure

As can be seen from the thin section results, the particle size of the reactive silica is too small to be resolved by optical microscope. Therefore, scanning electron microscope (SEM) under backscattered (BSE) mode is used to obtain the 2D microstructure of the limestone. Dried limestone samples were glued by epoxy and polished manually using a LaboPol-5 machine. Then 60 images were taken in five different samples using a JEOL scanning electron microscope equipped with an energy dispersive X-ray (EDX) spectroscopy detector operated at 15 kV with a magnification of 800x-1000x-2000x (image resolution of 1280x960 pixels).

Then, five representative images were selected for the 3D microstructure reconstruction. These images are chosen in such a way: Firstly, the quartz fractions in 60 images are calculated. The fractions were assumed to follow a normal distribution; Secondly, the minimum fraction, nearest to the true average fraction (13.21%) and maximum fraction were found. It was assumed that the minimum and maximum fraction is equal to -3δ and 3δ so that the standard deviation δ was calculated; Finally, the fraction near to [-3δ, -2δ , $-\delta$,0, δ , 2δ , 3δ] was found and used as our original images.

Figure 2.2 shows five representative SEM-BSE images of limestone. In a SEM-BSE image, phases with a higher atomic number scatter more electrons so that they are more brighter (with a high grey value) in the BSE image, while phases of lower atomic number absorb more electrons and are more darker (with a low grey value) in the BSE image. The grey value is positively related to the backscattering coefficient η, which is the fraction of scattered electrons. Based on this principle, in order to identify different phases on the BSE image, we calculated the backscattering coefficients for the minerals that discovered from XRD results (calcite, dolomite, fluorite, and quartz). The calculated coefficients for calcite, dolomite, fluorite, and quartz are 0.161, 0.143, 0.186 and 0.147 respectively. This means that in the image, the black part is pore, dark grey part is quartz while the light grey is other minerals.

It can be seen from the Figure 2.2 that most of the quartz particle size is between 1-10 μm. Most of the pore size is smaller than 1 μm, while some micro cracks are also discovered in some samples as shown in Image 2 of Figure 2.2. Because of the inherent noise in the images, a type of median filter is applied to smoothen the image. Here, each pixel is replaced by the majority phase present in a limited neighbourhood (e.g. 2x2) centred at the pixel. The phase at nanoscale is considered as noise and removed. Because the resolution in our model is set as 1 μm due to the computer calculation limitation, the images then were scaled to a resolution of 1 μm. This process will change the porosity or quartz

fraction depending on their particle size. A comparison of fraction before and after the image scaling was made as shown in Table 3.1. It can been seen that the quartz fractions are almost the same before and after image scaling while the porosity reduces a lot and almost reaches zero, which proves that most of the pores are at nanoscale while the quartz size is at microscale. Therefore, the reference parameter in this paper is the quartz fraction.

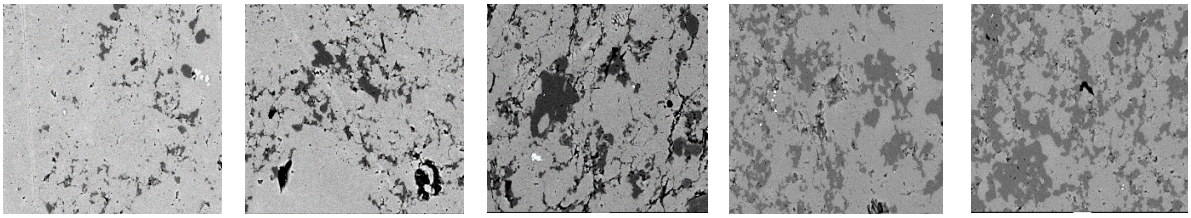

Image 1 Image 2 Image 3 Image 4 Image 5

Figure 2.2: Representative images of limestone in SEM-BSE images with different pore and quartz phase area fraction as shown in Table 2.2. The picture size is 1290x960 pixels with a scale of 0.1 μm per one pixel. (Black: pore; Dark grey: quartz; Light grey: other minerals).

Table 2.2: The phase fraction before and after image process.

	Pore,%		Quartz, %	
Image ID	Before	After	Before	After
1	0.155	0	7.36	6.83
2	1.933	0.77	12.45	12.38
3	2.729	0.0023	21.79	23.61
4	0.022	0	29.70	29.87
5	0.176	0.4	39.97	39.87

The five images after scaling were then binarized for pore and quartz respectively. The resulted binarized images of quartz are shown in Figure 2.3. These binarized images were then analysed to determine characteristic parameters that were utilized in reconstructing the 3D microstructures.

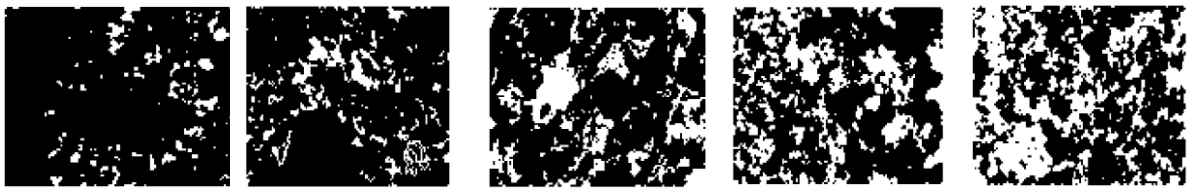

Image 1 Image 2 Image 3 Image 3 Image 4

Figure 2.3: Five representative images of limestone after filter, scaling and binarization. (White: quartz; Black: other minerals)

3. 3D MICROSTRUCTURE RECONSTRUCTION METHOD

3.1 Characterization used as input for the reconstruction

According to the Quiblier [8], a 2D image of a porous medium can be characterized by two functions:

(1) A probability distribution function (PDF) or the histogram of an image. This function is simply calculated by counting the number of the pixels located in the phase of interest and calculate the relative frequency respectively for each phase. From the PDF, the area fraction of each phase in the image can be easily calculated.

(2) An autocorrelation function (ACF). The "physical meaning'' of the ACF is a measure of the probability of finding two points a specific distance apart are both in the same phase.

The choice of these two functions (PDF and ACF) for characterizing a porous medium has been discusses by Joshi [13]. The most important fact is that they are among the few characteristics that remain unchanged two- or three-dimensionally. It should be noted that the porous medium does not need to be isotropic. An anisotropic ACF can be obtained by analysing several mutually perpendicular thin sections.

3.2 Description of the reconstruction process

Let $\mathrm{I(i,j)}$ be the value 1 or 0 depending on whether the point (i,j) is located in a pixel of phase s of interest or not. The probability function for an $\mathrm{M \cdot N}$ image is determined using Equation (1):

$$\mathrm{P(s)} = \frac{\sum_{i,j} I(i,j)}{M*N} \tag{1}$$

Where $\mathrm{s} = 1, 2$ for pore and quartz respectively in limestone in this paper.

The autocorrelation function of phase s is evaluated using the following Equation (2):

$$\mathrm{S_1(x,y)} = \sum_{i=1}^{M-x+1} \sum_{j=1}^{N-x+1} \frac{I(i,j)I(i+x-1,j+y-1)}{(M-x+1)(N-y+1)} \tag{2}$$

Where $\mathrm{(x,y)}$ is the point location and $1 \leq \mathrm{x} \leq \mathrm{M}, 1 \leq \mathrm{y} \leq \mathrm{N}$. To be more clear, $\mathrm{S_1(1,1)}$ is the probability of two pixels with a distance of 0 are in the same phase, which is actually the fraction of that phase on the image. $\mathrm{S_1(1,2)}$ is the probability that two pixels with a distance of 1 pixel at y axis are in the same phase, while $\mathrm{S_1(2,1)}$ is the probability that two pixels with a distance of 1 pixel at x axis are in the same phase.

One may recognize that Equation (2) is a convolution where the kernel is rotated 180° and as such, can be performed rapidly using Fourier transform methods to improve the calculation.

Given the two dimensional calculated $\mathrm{S_1(x,y)}$, we can obtain the desired one-dimensional or isotropic autocorrelation function $\mathrm{S_3(r)}$ by averaging over $\mathrm{S_1}$ values at a fixed radius r. $\mathrm{S_2(r,\theta)}$ value should be calculated through the Equation (3):

$$\mathrm{S_2(r,\theta)} = \mathrm{S_1}(r\cos\theta, r\sin\theta) \tag{3}$$

The value $\mathrm{S_1}(r\cos\theta, r\sin\theta)$ can be obtained by bilinear interpolation from the value of $\mathrm{S_1(x,y)}$.

Then $\mathrm{S_3(r)}$ can be given by Equation (4):

$$\mathrm{S_3(r)} = \frac{1}{2r+1} \sum_{l=0}^{2r} S_2\left(r, \frac{\pi l}{4r}\right) \tag{4}$$

Where $0 \leq \mathrm{r} \leq 256$. The maximum value of r is limited to 256 or less based on the experience of [8] and [11] as well as the statistical considerations.

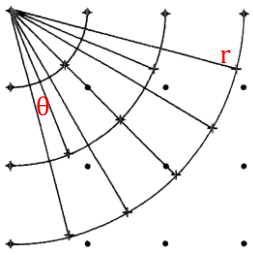

Figure 3.1: Illustration of algorithm for calculating $\mathrm{S_2(r,\theta)}$ and $\mathrm{S_3(r)}$ from the lattice points value $\mathrm{S_1(x,y)}$ for an image of interest, from Berryman [15].

After getting the one-dimensional autocorrelation function $\mathrm{S_3(r)}$, the 3D microstructure reconstruction can be achieved by three steps based on the research of [8] [11]:

(1) Generation of a random number $\mathrm{N(x,y,z)}$ at each point of the 100*100*100 domain following a normal distribution using the Box-Muller method [14]. The N numbers are completely uncorrelated. The initial phase at each point in this domain is considered as minerals except pore and quartz.

(2) For each point $(\mathrm{x},\mathrm{y},\mathrm{z})$, considering a neighbouring domain composed of points $(\mathrm{x}+\mathrm{r},\mathrm{y}+\mathrm{s},\mathrm{z}+\mathrm{t})$ up to a certain distance corresponding to the number of steps beyond which ACF becomes negligible (10 pixels in this paper). The values N in this neighbourhood are then linearly combined so as to form a new number denoted $\mathrm{R}(\mathrm{x},\mathrm{y},\mathrm{z})$ which is correlated and defined by equation (5). Periodic boundary condition is applied during the calculation of R.

$$\mathrm{R}(\mathrm{x},\mathrm{y},\mathrm{z}) = \sum_{r,s,t} F(r,s,t)\, N(x,y,z) \tag{5}$$

It has been proved [8] that the 3D ACF calculated from the 2D $\mathrm{S}_3(\mathrm{r})$ (Equation (6)) can be expressed as a function of the coefficient $F(r,s,t)$.

$$\mathrm{F}(\mathrm{r},\mathrm{s},\mathrm{t}) = \mathrm{F}(\mathrm{r}) = \frac{S_3\left(r=\sqrt{r+s^2+t^2}\right)-S_3(0)S_3(0)}{S_3(0)-S_3(0)S_3(0)} \tag{6}$$

(3) Finally, a threshold operation is performed on the filtered domain R to match the appropriate probability function from 2D for each phase of interest (the volume fraction is considered equal to the area fraction in this paper). The steps from (1) to (3) can be operated iteratively to separate all phases of interest.

According to Bentz [16], this simplified method will only approximate the CAF of the original microstructure, further modification may be required to adjust the CAF through adjusting the hydraulic radius of the interested phase. However, in this paper, the reconstructed CAF agrees very well to the true image when the range of [r, s, t] is set according to the true CAF and no further adjustment is needed.

4. VERIFICATION OF THE RECONSTRUCTED MICROSTRUCTURES

Five reconstructions has been done based on the binarized images. Two reconstructed 3D microstructure with a size of 100x100x100 $\mu\mathrm{m}$ with a quartz fraction of 6.83% (from image 1) and 39.87% (from image 5) are shown in Figure 4.1. The voxel size is 1 $\mu\mathrm{m}$. As stated before, probability function and autocorrelation are selected as the reference functions. Thus, the results can be checked in two ways: visual checking and numerical checking.

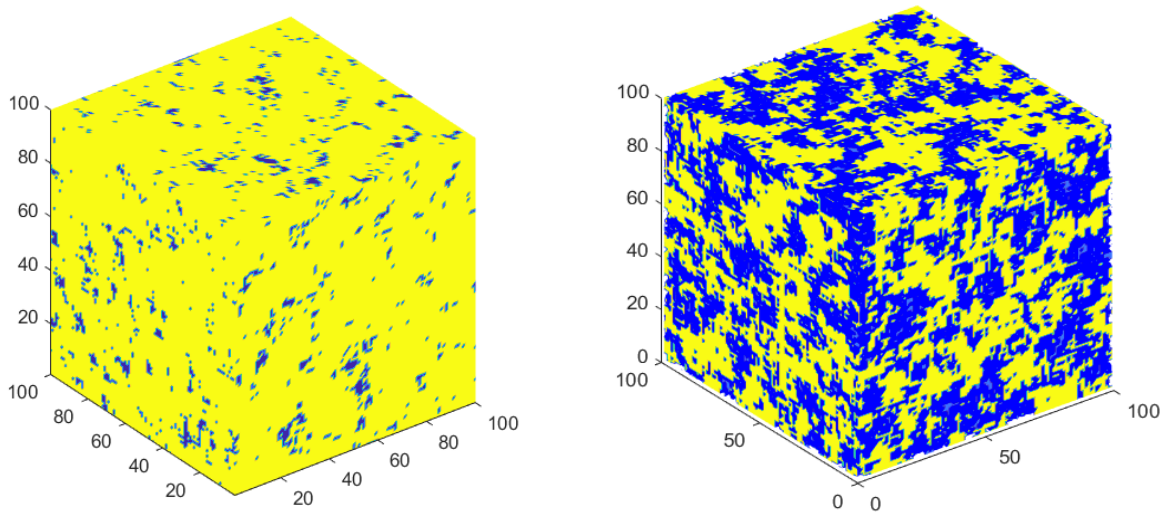

(a) Microstructure 1 (b) Microstructure 5

Figure 4.1: Reconstructed 3D microstructures. (a) Microstructure 1 with 6.83% of quartz; (b) Microstructure 5 with 39.87% of quartz. The blue part is quartz. The yellow part is the other minerals. The size of the domain is 100 x100x100 $\mu\mathrm{m}$ with a voxel size of 1 $\mu\mathrm{m}$.

4.1 Visual checking

Figure 4.2 shows six random slices from the simulated microstructure 1 and 5. At lower quartz fraction, the quartz particle sizes are smaller and distributed sparsely in the reconstructed model, which is similar to the original image. For higher quartz fraction, quartz particles are clustered together which makes the

structure more closely connected. This characteristic is also reconstructed relatively successful if one compares it with the original one. Therefore, to the naked eye, a similarity undoubtedly exists in shape, size and 'scattering' of quartz between the reconstructed microstructure and the real image.

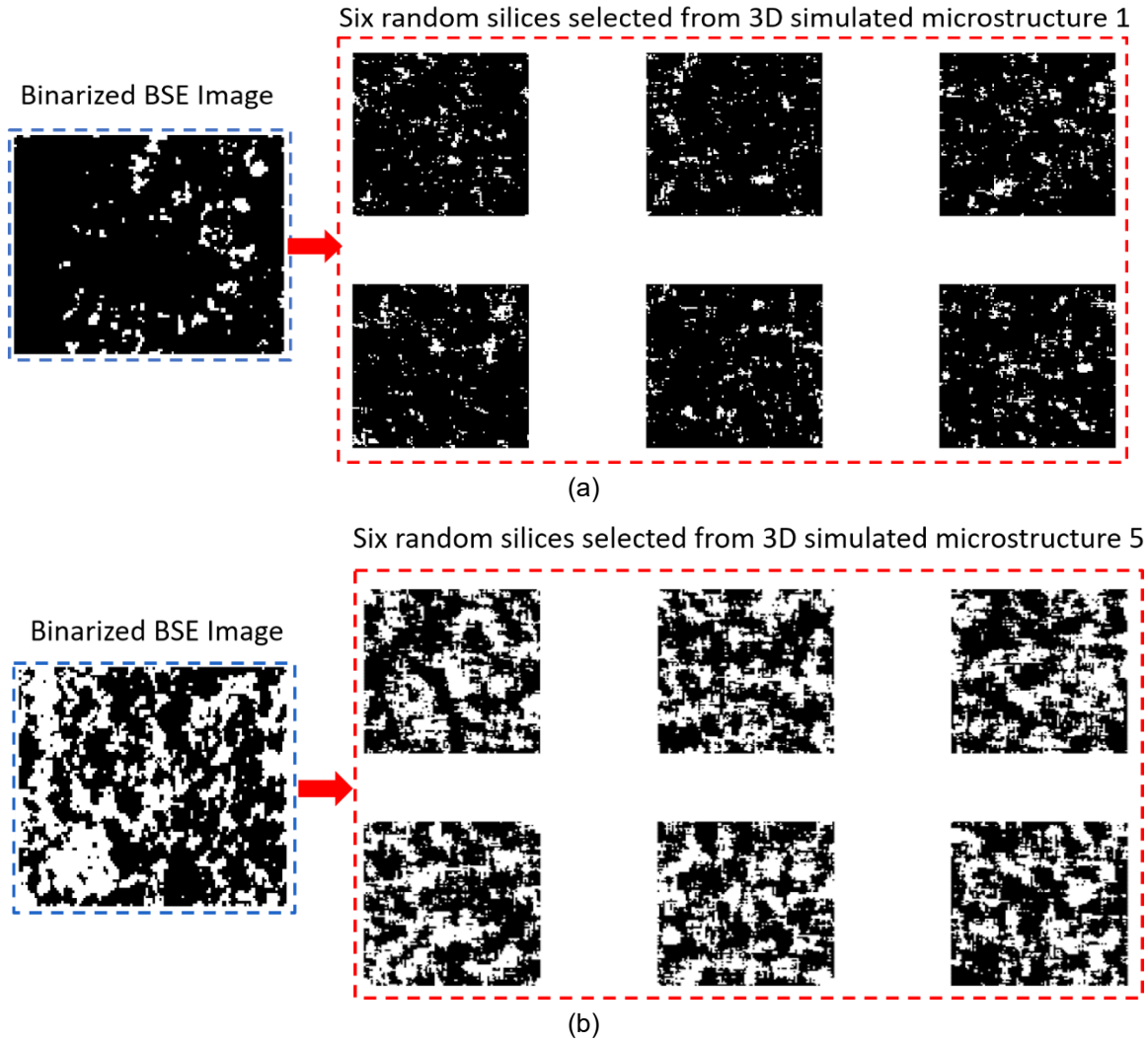

Figure 4.2: Random slices from the reconstructed microstructures. (a) Six random silices from the reconstructed microstructure 1 and its original binarized image; (b) Six random silices from the reconstructed microstructure 5 and its original binarized image 5. Image size is 100 x 100 um with a pixel size of 1 um. (White: quartz; Black: other minerals).

4.2 Numerical checking

As the phase fraction (PDF) is already fitted through the threshold filtration during the reconstruction, we only compute the ACF of the reconstructed microstructures and compare them to those of the real medium (Figure 4.2). Here, the ACF curve of the original image was computed from the original 2D binarized image, while the reconstructed ACF curve was computed for the entire newly constructed 3D microstructures.

The original and reconstructed ACF are seen to nearly overlap in the distance range of a value from 0 to around 10 pixels in all of the microstructures as seen in Figure 4.3. At a longer distance, the curves no longer overlap due to the extent of the filter operation used during the generation algorithm (10 pixels) or the random nature of the starting Gaussian noise image as also found in [16].

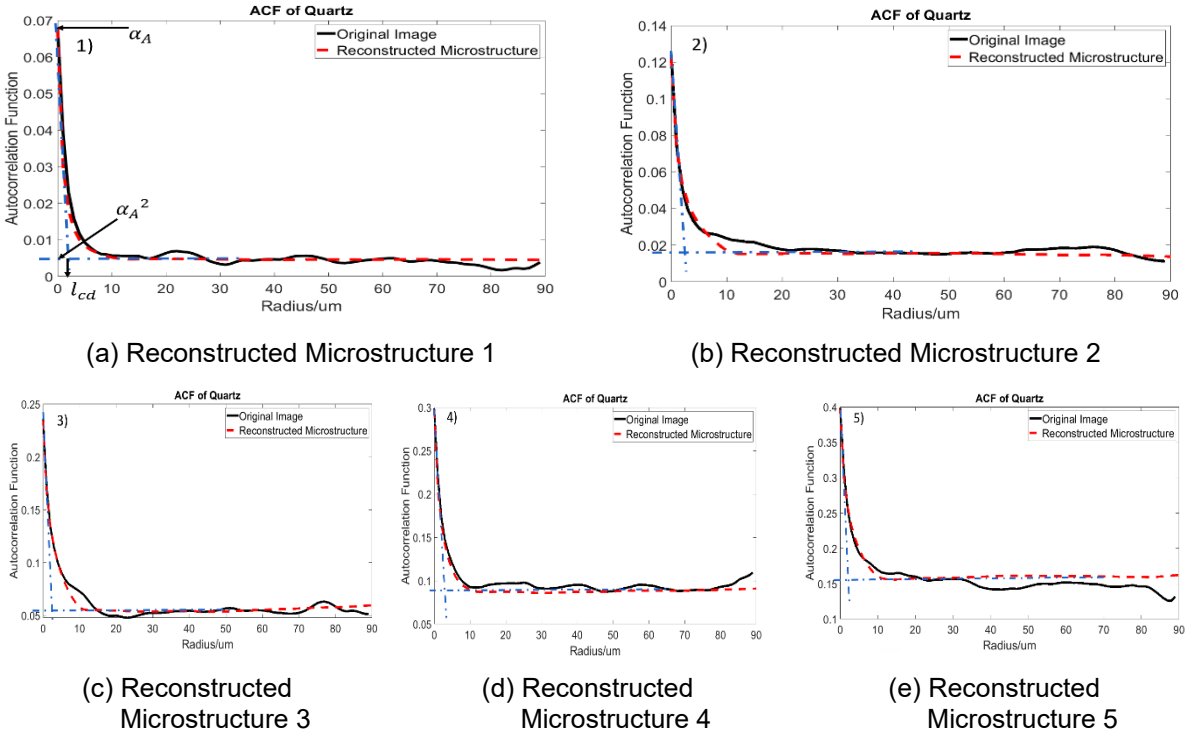

(a) Reconstructed Microstructure 1

(b) Reconstructed Microstructure 2

(c) Reconstructed Microstructure 3

(d) Reconstructed Microstructure 4

(e) Reconstructed Microstructure 5

Figure 4.3: Autocorrelation function(ACF) of quartz from the original image and the reconstructed microstructures.

As stated before, the ACF describes the probability of two random points with a distance 'r' located in the same phase. It contains information about the area fraction, characteristic particle size and the specific surface area of the phase of interest. Take the ACF of the original image 1 as shown in Figure 4.3 (a) as an example. The value of the ACF at r=0 corresponds to the quartz area fraction (volume fraction for the red line) of the image 1 (α_A). The plateaus value of the function correspond to the α_A^2. The intersection of the slope of ACF at r=0 and the plateau region indicates a characteristic dimension of the quartz structure. The slope of the ACF at r=0 relates to the specific surface area of the quartz. By comparing the ACF curves in Figure 4.3, we can say that all three parameters of the constructed microstructure match very well with that of the original image. The striking visual similarity and well-fitting of the ACF for the distance up to 10 pixels shows that this method has a good ability to reconstruct the real 3D microstructure based on the 2D image.

5. APPLICATION OF THE MODEL

The main purpose of simulating the 3D microstructure for the aggregate is to use it as a basis in a multiscale ASR simulation model. More specifically, the simulated microstructure of the siliceous limestone can be used to simulate the pore solution ions transportation, the dissolution of the reactive silica, the nucleation and growth of ASR products as well as the following cracking process induced by ASR beginning from the microscale, which is more consistent with the actual situation. Then, based on the multiscale fracture modelling technique in [18], by passing the mechanical simulation results to a higher scale the cracking process of the concrete at mesoscale or macroscale can also be simulated.

Compared with other models, the output of such a model is variable. At microscale, the evolution of the alkalis, the pH of the pore solution and the microstructure of the cement paste and aggregate under the attack of ASR can be traced. The effects of different influencing factors, such as the concentration of calcium ions or the temperature and so on, on the evolution of the ASR products and the expansion sites can be explored. What's more, the cracking process at microscale can be also simulated. While at mesoscale or macroscale, the expansion of the structure, the pessimum size of the aggregate, the mechanical degradation as well as the fracture mechanism can be obtained. Such a model will be illustrated in our next paper.

6. CONCLUSION

A very reactive limestone in Belgium was analysed and the Gaussian filtering method based on [8] and [16] to reconstruct the 3D microstructure from 2D image was followed in this paper. In the limestone, the ASR reactive silica is mainly microcrystalline to cryptocrystalline quartz as confirmed by the thin section and SEM and the average mass of the reactive fraction is around 13.21%. On the other hand, the pore size in this aggregate is mainly below 1 μm while the quartz size is mainly between 1 μm and 10 μm. Five kind of microstructures of the limestone with quartz fraction from 6.83% to 39.87% of the limestone were simulated using the Gaussian filtration method. The comparison of the 2D slice structure and ACF functions between the original 2D image and reconstructed microstructures shows that the reconstructed 3D limestone retains the visual characteristics (such as the particle shape and spatial scattering), as well as the statistical characteristics (such as the area fraction, characteristic particle size and the specific surface area) of the quartz of the parent limestone. The resulted microstructures can be used as one of the input in a ASR multiscale model to simulate the chemical reaction (such as dissolution of the reactive quartz, the nucleation and growth of the ASR products) and physical response at microscale.

7. REFERENCES

[1] Rajabipour F, Giannini E, Dunant C, Ideker JH, Thomas MD (2015) Alkali–silica reaction: Current understanding of the reaction mechanisms and the knowledge gaps. Cem Concr Res 76:130-146. https://doi.org/10.1016/j.cemconres.2015.05.024

[2] Ponce JM, Batic OR (2006) Different manifestations of the alkali-silica reaction in concrete according to the reaction kinetics of the reactive aggregate. Cem Concr Res 36(6):1148-1156. https://doi.org/10.1016/j.cemconres.2005.12.022

[3] Leemann A, Münch B (2019) The addition of caesium to concrete with alkali-silica reaction: Implications on product identification and recognition of the reaction sequence. Cem Concr Res 120:27-35. https://doi.org/10.1016/j.cemconres.2019.03.016

[4] Bažant ZP, Steffens A (2000). Mathematical model for kinetics of alkali–silica reaction in concrete. Cem Concr Res 30(3):419-428. https://doi.org/10.1016/S0008-8846(99)00270-7

[5] Wang Y, Meng Y, Jiradilok P, Matsumoto K, Nagai K, Asamoto S (2019) Expansive cracking and compressive failure simulations of ASR and DEF damaged concrete using a mesoscale discrete model. Cem Concr Compos 104: 103404. https://doi.org/10.1016/j.cemconcomp.2019.103404

[6] Dunant CF, Scrivener KL (2010) Micro-mechanical modelling of alkali–silica-reaction-induced degradation using the AMIE framework. Cem Concr Res 40(4):517-525. https://doi.org/10.1016/j.cemconres.2009.07.024

[7] Esposito R, Hendriks MAN (2019) Literature review of modelling approaches for ASR in concrete: a new perspective. Eur J Environ Civ Eng 23(11):1311-1331. https://doi.org/10.1080/19648189.2017.1347068

[8] Quiblier JA (1984) A new three-dimensional modelling technique for studying porous media. J Colloid Interface Sci 98:84-102. https://doi.org/10.1016/0021-9797(84)90481-8

[9] Biswal B, Manswarth C, Hilfer R, Bakke S, Oren PE (1999) Quantitative analysis of experimental and synthetic microstructure for sedimentary rocks. Physica A273:452-475. https://doi.org/10.1016/S0378-4371(99)00248-4

[10] Zhao XZ, Yao J, Yi YJ (2007) A new stochastic method of reconstructing porous media. Transp Porous Med 69(1):1-11. https://doi.org/10.1007/s11242-006-9052-9

[11] Bentz DP (1997) Three-dimensional computer simulation of Portland cement hydration and microstructure development. J Am Ceram Soc 80(1):3-21. https://doi.org/10.1111/j.1151-2916.1997.tb02785.x

[12] EN 932-2 (1999) Tests for general properties of aggregates. Methods for reducing laboratory samples. Brussels, Belgium.

[13] Joshi M (1974) A class of stochastic models for porous media. Dissertation. University of Kansas.

[14] Law AM, Kelton WD (1982) Simulation modelling and analysis. McGraw-Hill, New York.

[15] Berryman JG (1985) Measurement of spatial correlation functions using image processing techniques. Journal of applied physics 57:2374. https://doi.org/10.1063/1.334346

[16] Bentz DP, Martys NS (1994) Hydraulic radius and transport in reconstructed model three-dimensional porous media. Transp Porous Med 17:221-238. https://doi.org/10.1007/BF00613583

[17] Fernandes I, Ribeiro MDA, Broekmans MA, Sims I (2016) Petro-graphic Atlas: Characterisation of aggregates regarding potential reactivity to alkalis: RILEM TC 219-ACS recommended guidance AAR-1.2, for use with the RILEM AAR-1.1 Petrographic examination method. Berlin, Germany.

[18] Qian ZW (2012) Multiscale modelling of fracture processes in cementitious materials. Dissertation, Delft University of Technology.

[19] De Schutter G (2013) The detrimental power of alkali silica reaction: remarkable case study. In Concrete under Severe Conditions: Environment and Loading (CONSEC-2013) (Vol. 2, pp.1229-1242). RILEM Publications SARL.

[20] MacKenzie WS, Adams A E, Brodie KH (2017) Rocks and minerals in thin section: A colour atlas. Florida, USA.